

# Multi-frequency sparse Bayesian learning with uncertainty models

Santosh Nannuru, Kay L. Gembä, Peter Gerstoft, William S. Hodgkiss, Christoph Mecklenbräuker

**Abstract**—Sparse Bayesian learning (SBL) has emerged as a fast and competitive method to perform sparse processing. The SBL algorithm, which is developed using a Bayesian framework, approximately solves a non-convex optimization problem using fixed point updates. It provides comparable performance and is significantly faster than convex optimization techniques used in sparse processing. In this paper we propose signal model which accounts for dictionary mismatch and the presence of spurious peaks at low signal-to-noise ratios. As an extension of SBL, modified fixed point update equation is derived which incorporates the statistics of mismatch and spurious peaks. We also extend the SBL algorithm to process multi-frequency observations. The derived update equations are studied quantitatively using beamforming simulations applied to direction-of-arrival (DoA) estimation. Performance of SBL using single frequency and multi-frequency observations, and in the presence of aliasing is evaluated. Data collected from the SwellEx-96 experiment is used to demonstrate qualitatively the advantages of SBL.

**Index Terms**—Sparse Bayesian learning, sparse signal processing, compressive sensing, beamforming, direction of arrival estimation, multi frequency, aliasing, wide band

## I. INTRODUCTION AND MOTIVATION

Compressed sensing or sparse processing is the process of estimating sparse vectors using significantly fewer measurements. Mathematically, this corresponds to solving an underdetermined system of linear equations under the constraint that the solution is sparse. The exact solution has combinatorial complexity which is impractical to solve for high dimensional problems. The most popular, approximate and computationally feasible, sparse processing method is basis pursuit [1] implemented using the LASSO [2] algorithm. Basis pursuit relaxes the sparsity criteria and the solution is given by solving a convex optimization problem. Though feasible, solving the optimization problem for high dimensions is still computationally slow. One of the faster alternatives is the matching pursuit algorithm [3]. But matching pursuit is a greedy approach and can lead to suboptimal support detection. Another alternative which is not greedy and is significantly faster than basis pursuit is sparse Bayesian learning (SBL) [4]–[10].

In SBL, the sparse weight vector in the underdetermined system of linear equations is treated as a random vector with Gaussian prior. Explicit sparsity constraints are not imposed on the weight vectors. Unlike traditional prior models, the

Santosh Nannuru, Kay L. Gembä, Peter Gerstoft, and William S. Hodgkiss are with the Scripps Institution of Oceanography at University of California, San Diego; snannuru@ucsd.edu, kgembä@ucsd.edu, pgerstoft@ucsd.edu, and whodgkiss@ucsd.edu.

Christoph Mecklenbräuker is with Institute of Telecommunications, Vienna University of Technology, 1040 Vienna, Austria, cfm@ieee.org.

parameters of the Gaussian prior are assumed unknown and are estimated by performing evidence (i.e. data likelihood) maximization. The objective function for performing evidence maximization is non-convex and an approximate solution is obtained by formulating a fixed point update equation. The solution at convergence gives a parameter estimate which is sparse and hence the weight vectors are also sparse.

A significant advantage of SBL over basis pursuit is that it can determine automatically the sparsity without any user input. Being a probabilistic approach, SBL computes the posterior distribution of the sparse weight vectors and hence provides estimates of their covariance along with the mean. Computationally, SBL can significantly outperform LASSO [10].

Most of the existing literature on sparse processing assumes that the sensing matrix or dictionary is deterministic and completely known. This is not feasible in many practical applications, some of which include beamforming [11], [12] and matched-field processing [13], [14]. Also, at low signal-to-noise ratio (SNR), the identified solution can contain many false or spurious entries not present in the true sparse solution. These false entries often mask true sparse entries and introduce errors in parameter estimation.

The three main contributions of this work are the following:

**1) Multi-frequency multi-snapshot SBL:** We derive an SBL algorithm for multiple snapshots using a fixed-point update [10]. This gives unbiased noise estimates and has better convergence properties especially for high SNR [10]. We then consider multi-frequency observations, which are combined assuming either constant or varying power across frequency. Combining multiple frequencies within SBL provides a processing gain especially at low SNR and reduces aliasing when the signal is insufficiently sampled spatially.

**2) Modifications to SBL:** We propose modifications to SBL to address sensing matrix mismatch and to reduce spurious errors in the weight vector which occur in presence of noise. The linear-Gaussian signal model is modified and transformed into a linear non-Gaussian model. We make approximations so that the model remains linear-Gaussian and hence the regular SBL methodology can be applied. We focus on statistical modeling and integrating out of the error parameters rather than their estimation. This approach has the advantage that a large class of errors can be modeled and the resulting algorithm has a simple formulation.

**3) Simulations and real data analysis:** The proposed algorithms are demonstrated and verified using beamforming simulations for estimating direction-of-arrivals (DoA) of multiple plane waves. Data from the SwellEx-96 experiment demonstrates application to real data and its ability to reduce

aliasing when processing multiple frequencies.

The remainder of the paper is organized as follows. A detailed review of related literature is provided in Section I-A. The signal model along with assumptions on priors and likelihoods are discussed in Section II. The modified SBL algorithm is derived in Section III along with its multi-frequency extension. The derived algorithms are studied using simulations and real data in Section IV. Conclusions are provided in Section V.

### A. Related literature

SBL was first introduced by Tipping [4] for regression and classification problems in the context of machine learning. It has been used since in the signal processing literature [5], [7] with various modifications and extensions [6], [8], [9].

Since SBL does not explicitly impose any sparsity constraints but is able to determine sparsity automatically, various explanations have been discussed. It is argued in [15], [16] that the SBL solution can be obtained by solving an iterated reweighted LASSO problem and hence sparsity can be expected. In [17] it is shown that under certain conditions on the sensing matrix, SBL can identify sparse solutions without any explicit sparsity constraints. Cramer-Rao bounds for SBL solution are discussed in [18]. Various sparse signal recovery solutions including LASSO and SBL are unified within the Bayesian framework in [19]. We also make note of approximate message passing based algorithms in [20] and [21], which also utilize a Bayesian framework, to solve the underdetermined linear problem.

Beamforming can be used to estimate the DoAs of multiple plane waves from sensor array observations. By formulating beamforming as an underdetermined linear problem, compressed sensing has been applied to estimate DoAs in [11], [12], [22]. The problem of mismatch and robustness of traditional beamforming algorithms has been studied extensively [23]–[27].

Perturbations and mismatch also have been addressed in compressed sensing literature for basis pursuit [13], [28], [29], matching pursuit [30], and approximate message passing [31]. For SBL, beamforming in the presence of array imperfections is addressed in [32], [33]. Robustness of SBL to outliers in image processing application is studied in [34].

### B. Notations

We briefly explain the mathematical notations used throughout this paper. Scalar quantities are denoted by lowercase letters. Lowercase bold alphabets denote vectors and uppercase bold alphabets denote matrices. A vector or matrix of all zeros is denoted by  $\mathbf{0}$  where appropriate dimensions are assumed. Similarly a vector or matrix of all ones is denoted by  $\mathbf{1}$ . An identity matrix of dimension  $N \times N$  is denoted  $\mathbf{I}_N$ . The notation  $\mathbf{M}^H$  denotes the Hermitian (conjugate transpose) operation performed on a complex valued matrix  $\mathbf{M}$ . The transpose operation on  $\mathbf{M}$  is denoted  $\mathbf{M}^T$ . The field of complex numbers is denoted  $\mathbb{C}$ .

## II. SIGNAL MODEL

In this section, we discuss the signal model used in SBL and the assumptions made in this paper. Let  $\mathbf{y} \in \mathbb{C}^N$  be the complex signal which is expressed as

$$\mathbf{y} = \mathbf{Ax} + \mathbf{n}, \quad (1)$$

where the noise  $\mathbf{n} \in \mathbb{C}^N$  is zero mean circularly symmetric complex Gaussian (Appendix A) with covariance matrix  $\sigma^2 \mathbf{I}_N$ ;  $\mathbf{I}_N$  is an  $N \times N$  identity matrix;  $\mathbf{A} \in \mathbb{C}^{N \times M}$  is the sensing matrix;  $\mathbf{x} \in \mathbb{C}^M$  is the weight vector. In sparse problem formulations,  $\mathbf{x}$  is assumed sparse with at most  $K$  non-zero entries where  $K \ll M$ . Sparsity level  $K$  is not required explicitly or modeled by SBL. The vector  $\mathbf{x}$  acts as a selection operator identifying columns of  $\mathbf{A}$  that best explain the signal  $\mathbf{y}$ . We assume  $\mathbf{A}$  has the maximal column rank  $N$ .

*Error in sensing matrix:* Often  $\mathbf{A}$  is assumed known. This does not hold when there is uncertainty in the model or parameters used to construct  $\mathbf{A}$ . For example, in plane wave beamforming entries of  $\mathbf{A}$  depend on array positions and signal speed of propagation. These parameters may be uncertain or can change over time. To account for perturbations we express

$$\mathbf{A} = \mathbf{A}^o + \mathbf{A}^e, \quad (2)$$

where  $\mathbf{A}^o$  is known and  $\mathbf{A}^e$  is a random perturbation matrix. The perturbation (2) has been studied in [13], [27]–[30], [35]. In the context of beamforming, sensing matrix perturbations have been studied in [24], [32]. An example where multiplicative noise gives rise to such perturbations in the sensing matrix is discussed in Appendix C. Though the component  $\mathbf{A}^e$  is random and unknown, its statistics are known. The prior model for  $\mathbf{A}^e$  is discussed in Section II-A.

*Error in weights:* We assume  $\mathbf{x}$  consists of two components

$$\mathbf{x} = \mathbf{x}^o + \mathbf{x}^e, \quad (3)$$

where the first component  $\mathbf{x}^o$  is sparse and the second component  $\mathbf{x}^e$  may be sparse. The component  $\mathbf{x}^e$  accounts for spurious or false peaks arising due to noise or modeling mismatch. Here both  $\mathbf{x}^o$  and  $\mathbf{x}^e$  are random and their prior models are discussed in Section II-A.

The vector  $\mathbf{x}^o$  consists of complex amplitudes of the true sources (which is sparse when there are few sources). The vector  $\mathbf{x}^e$  is composed of the spurious peaks in  $\mathbf{x}$  due to noise or modeling mismatch. Likely  $\mathbf{x}^e$  is sparse but we cannot uniquely distinguish the support of  $\mathbf{x}^e$  from that of  $\mathbf{x}^o$ . Also, given that the source locations are stationary, the support of  $\mathbf{x}^e$  might vary because the noise realization changes over time. To overcome this limitation we assume that the statistics of  $\mathbf{x}^e$  is known without knowledge of its support.

*Modified signal model:* Including the perturbed quantities from (2) and (3), the signal model (1) is modified as

$$\mathbf{y} = \mathbf{Ax} + \mathbf{n} = (\mathbf{A}^o + \mathbf{A}^e)(\mathbf{x}^o + \mathbf{x}^e) + \mathbf{n} \quad (4)$$

$$= \mathbf{A}^o \mathbf{x}^o + \mathbf{A}^e \mathbf{x}^o + \mathbf{A}^o \mathbf{x}^e + \mathbf{A}^e \mathbf{x}^e + \mathbf{n} \quad (5)$$

where the first and the last terms on right hand side are the regular linear model in SBL. The terms  $\mathbf{A}^e \mathbf{x}^o$ ,  $\mathbf{A}^o \mathbf{x}^e$  and  $\mathbf{A}^e \mathbf{x}^e$  are additional “noise” terms. To focus on only one kind

of error we set either  $\mathbf{A}^e = \mathbf{0}$  or  $\mathbf{x}^e = \mathbf{0}$ . We develop our theory for the general case and consider individual cases in the simulations. Setting both  $\mathbf{A}^e$  and  $\mathbf{x}^e$  to zero gives the regular SBL signal model (1). We assume  $\mathbf{x}^o$ ,  $\mathbf{x}^e$ ,  $\mathbf{A}^e$ , and  $\mathbf{n}$  are mutually independent. Since later in simulations section we consider either  $\mathbf{A}^e = \mathbf{0}$  or  $\mathbf{x}^e = \mathbf{0}$ , the independence assumption of  $\mathbf{x}^e$  and  $\mathbf{A}^e$  is not crucial for our analysis.

### A. Prior models

*Prior model for  $\mathbf{x}^o$ :* In SBL  $\mathbf{x}^o$  is modeled as a zero mean circularly symmetric complex Gaussian with prior density  $p(\mathbf{x}^o) = \mathcal{CN}(\mathbf{x}^o; \mathbf{0}, \mathbf{\Gamma})$ , where the unknown covariance matrix  $\mathbf{\Gamma}$  is assumed diagonal,  $\mathbf{\Gamma} = \text{diag}(\boldsymbol{\gamma})$ ,  $\boldsymbol{\gamma} = [\gamma_1 \dots \gamma_M]$ . See Appendix A for definition of the complex Gaussian density function. The covariance  $\mathbf{\Gamma}$  is unknown and estimated by SBL.

We assume the error terms  $\mathbf{x}^e$  and  $\mathbf{A}^e$  are stochastic and define statistics over them. These statistics easily integrate all possible error realizations while computing evidence and allows us to study their effect on average. An alternate approach could be to estimate  $\mathbf{x}^e$  and  $\mathbf{A}^e$  from data but that would significantly increase the dimensionality of the problem. Hence we do not pursue this approach.

*Prior model for  $\mathbf{x}^e$ :* The term  $\mathbf{x}^e$  was introduced to account for false peaks. We model  $\mathbf{x}^e$  to have zero mean and covariance matrix  $\mathbf{\Gamma}^e$ , the relation matrix is assumed zero. The covariance matrix  $\mathbf{\Gamma}^e$  is diagonal and known,  $\mathbf{\Gamma}^e = \text{diag}(\boldsymbol{\gamma}^e)$ . It quantifies the prior knowledge of errors in  $\mathbf{x}$ . We can choose  $\boldsymbol{\gamma}^e$  empirically based on the specific application. The term  $\mathbf{x}^e$  establishes a noise floor for  $\mathbf{x}$  and helps in strengthening weaker peaks (see simulations in Section IV). In this sense it is similar to the concept of stochastic resonance [36], [37] where adding noise into a non-linear system improves its detection performance.

*Prior model for  $\mathbf{A}^e$ :* Let  $p(\mathbf{A}^e)$  be the density function of the error matrix  $\mathbf{A}^e = [\mathbf{a}_1^e \dots \mathbf{a}_M^e]$ . For computational tractability we impose certain restrictions on  $\mathbf{A}^e$ . We assume that the  $m$ th column  $\mathbf{a}_m^e$  has known covariance matrix  $\mathbf{\Sigma}_m^e$ . No assumption is made about the mean. Also, let the columns of  $\mathbf{A}^e$  be statistically orthogonal. Hence

$$E(\mathbf{a}_m^e \mathbf{a}_n^{eH}) = \delta(m - n) \mathbf{\Sigma}_m^e \quad (6)$$

(Note: Here we have relaxed the Gaussian and zero-mean assumption on  $\mathbf{A}^e$ . The second moment  $\mathbf{\Sigma}_m^e$  contains both covariance and mean information.)

In [13] the perturbation vectors  $\mathbf{a}_m^e$  are assumed stochastic and an elastic net regression is formulated by averaging out the perturbations. The perturbations are assumed to be complex Gaussian random vectors in [27]. Parametric modeling of the perturbations  $\mathbf{a}_m^e$  is considered in [32] for plane wave beamforming. The parameters are estimated within the iterative framework of SBL but only specific perturbations are considered and cannot be generalized to include a broader class of errors.

### B. Likelihood

Combining all the “noise” terms together gives

$$\mathbf{y} = \mathbf{A}^o \mathbf{x}^o + \mathbf{A}^e \mathbf{x}^e + \mathbf{A}^o \mathbf{x}^e + \mathbf{A}^e \mathbf{x}^o + \mathbf{n} \quad (7)$$

$$= \mathbf{A}^o \mathbf{x}^o + \boldsymbol{\eta} \quad (8)$$

where  $\boldsymbol{\eta} = \mathbf{A}^e \mathbf{x}^o + \mathbf{A}^o \mathbf{x}^e + \mathbf{A}^e \mathbf{x}^e + \mathbf{n}$ . Here  $\boldsymbol{\eta}$  can be considered as the modified noise term which depends on  $\mathbf{x}^o$ ,  $\mathbf{A}^o$ ,  $\mathbf{x}^e$ ,  $\mathbf{A}^e$ , and  $\mathbf{n}$ . Since  $\mathbf{n}$  is Gaussian, given the total weight vector  $\mathbf{x} = \mathbf{x}^o + \mathbf{x}^e$  and the total sensing matrix  $\mathbf{A} = \mathbf{A}^o + \mathbf{A}^e$ , the likelihood function for the model in (5) and (8) is

$$p(\mathbf{y}|\mathbf{x}) = p(\mathbf{y}|\mathbf{x}; \mathbf{A}) = \mathcal{CN}(\mathbf{y}; \mathbf{Ax}, \sigma^2 \mathbf{I}_N). \quad (9)$$

The modified noise  $\boldsymbol{\eta}$  is not Gaussian since  $\boldsymbol{\eta}$  is composed of terms  $\mathbf{A}^e$  and  $\mathbf{x}^e$  whose densities are not known in general (from the prior models in Section II-A). To move forward within the SBL framework, we approximate  $\boldsymbol{\eta}$  to be Gaussian. Note that a Gaussian assumption on the variables  $\mathbf{A}^e$  and  $\mathbf{x}^e$  will still not simplify the distribution of  $\boldsymbol{\eta}$  as the terms  $\mathbf{A}^e \mathbf{x}^o$  and  $\mathbf{A}^e \mathbf{x}^e$  will involve products of Gaussian random variables which do not have simplified closed form distributions.

*Approximate likelihood:* To simplify the likelihood model, we compute the mean and covariance of  $\boldsymbol{\eta}$ :

$$E(\boldsymbol{\eta}) = E(\mathbf{A}^e \mathbf{x}^o + \mathbf{A}^o \mathbf{x}^e + \mathbf{A}^e \mathbf{x}^e + \mathbf{n}) = \mathbf{0} \quad (10)$$

$$\begin{aligned} \Sigma_{\boldsymbol{\eta}} = E(\boldsymbol{\eta} \boldsymbol{\eta}^H) &= E(\mathbf{A}^e \mathbf{x}^o \mathbf{x}^{oH} \mathbf{A}^{eH}) + E(\mathbf{A}^o \mathbf{x}^e \mathbf{x}^{eH} \mathbf{A}^{oH}) \\ &\quad + E(\mathbf{A}^e \mathbf{x}^e \mathbf{x}^{eH} \mathbf{A}^{eH}) + E(\mathbf{n} \mathbf{n}^H) \end{aligned} \quad (11)$$

$$\begin{aligned} &= \sum_{m,n} \left[ E(x_m^o x_n^{oH}) E(\mathbf{a}_m^e \mathbf{a}_n^{eH}) + E(x_m^e x_n^{eH}) \mathbf{a}_m^o \mathbf{a}_n^{oH} \right. \\ &\quad \left. + E(x_m^e x_n^{eH}) E(\mathbf{a}_m^e \mathbf{a}_n^{eH}) \right] + \sigma^2 \mathbf{I}_N \end{aligned} \quad (12)$$

$$= \sum_m \left[ \gamma_m \mathbf{\Sigma}_m^e + \gamma_m^e \mathbf{a}_m^o \mathbf{a}_m^{oH} + \gamma_m^e \mathbf{\Sigma}_m^e \right] + \sigma^2 \mathbf{I}_N \quad (13)$$

We have used the mutual independence of  $\mathbf{x}^o$ ,  $\mathbf{x}^e$ ,  $\mathbf{A}^e$ , and  $\mathbf{n}$  in above simplification. While computing the covariance of  $\boldsymbol{\eta}$ , the error terms  $\mathbf{x}^e$  and  $\mathbf{A}^e$  are integrated out and the covariance matrix  $\Sigma_{\boldsymbol{\eta}}$  depends on their statistics  $\boldsymbol{\gamma}^e$ ,  $\mathbf{\Sigma}_m^e$  along with  $\gamma$  and  $\sigma^2$ . This integration circumvents the need to explicitly estimate the unknowns  $\mathbf{x}^e$  and  $\mathbf{A}^e$ .

For analytical simplification, we approximate the density of  $\boldsymbol{\eta}$  to be Gaussian with mean zero and covariance  $\Sigma_{\boldsymbol{\eta}}$

$$p(\boldsymbol{\eta}) \approx \mathcal{CN}(\boldsymbol{\eta}; \mathbf{0}, \Sigma_{\boldsymbol{\eta}}). \quad (14)$$

To justify this approximation expand the modified noise as:  $\boldsymbol{\eta} = \sum_m (x_m^o \mathbf{a}_m^e + x_m^e \mathbf{a}_m^o + x_m^e \mathbf{a}_m^e) + \mathbf{n}$ . Thus  $\boldsymbol{\eta}$  is a sum of large number of random vectors. From the central limit theorem,  $\boldsymbol{\eta}$  converges to a Gaussian distribution as  $M \rightarrow \infty$ . When  $\mathbf{x}^o$  is  $K$ -sparse, the error in the Gaussian approximation (14) decreases with  $\frac{1}{\sqrt{K}}$ . The likelihood for the signal model (8) is approximately

$$p(\mathbf{y}|\mathbf{x}^o) = p(\mathbf{y}|\mathbf{x}^o; \mathbf{A}^o) \approx \mathcal{CN}(\mathbf{y}; \mathbf{A}^o \mathbf{x}^o, \Sigma_{\boldsymbol{\eta}}). \quad (15)$$

Note that once the modified noise  $\boldsymbol{\eta}$  is approximated as Gaussian, we treat  $\boldsymbol{\eta}$  and  $\mathbf{x}^o$  as independent (which is not necessarily true from the expression for  $\boldsymbol{\eta}$  which depends on  $\mathbf{x}^o$ ). This assumption is necessary to evaluate analytically the evidence in Section III-A.

### C. Multiple snapshots

To increase the SNR, we process multiple observations (snapshots) simultaneously. Let  $\mathbf{Y} = [\mathbf{y}_1 \dots \mathbf{y}_L] \in \mathbb{C}^{N \times L}$  denote  $L$  consecutive snapshots arranged column wise in a matrix. The multi snapshot analogue of (1) is

$$\mathbf{Y} = \mathbf{A}^o \mathbf{X}^o + \underline{\boldsymbol{\eta}} \quad (16)$$

where  $\mathbf{X}^o = [\mathbf{x}_1^o \dots \mathbf{x}_L^o]$  and  $\underline{\boldsymbol{\eta}} = [\underline{\boldsymbol{\eta}}_1 \dots \underline{\boldsymbol{\eta}}_L]$ . The  $\mathbf{x}_l^o$  are assumed i.i.d. Gaussian across snapshots

$$p(\mathbf{X}^o) = \prod_{l=1}^L p(\mathbf{x}_l^o) = \prod_{l=1}^L \mathcal{CN}(\mathbf{x}_l^o; \mathbf{0}, \boldsymbol{\Gamma}). \quad (17)$$

The error terms  $\mathbf{A}^e$ ,  $\mathbf{x}^e$ , and the noise  $\mathbf{n}$  are assumed independent across snapshots. The multi snapshot likelihood is

$$p(\mathbf{Y}|\mathbf{X}^o) = \prod_{l=1}^L p(\mathbf{y}_l|\mathbf{x}_l^o; \mathbf{A}^o) \quad (18)$$

where single snapshot likelihood  $p(\mathbf{y}_l|\mathbf{x}_l^o; \mathbf{A}^o)$  is from (15).

### D. Multiple frequencies (wideband)

To improve estimation accuracy, multiple frequencies are processed together. Let the observation vectors recorded at  $F$  frequencies be denoted by  $\mathbf{Y}_1 \dots \mathbf{Y}_F$  with the corresponding sparse weight vectors  $\mathbf{X}_1^o \dots \mathbf{X}_F^o$ . We have

$$\mathbf{Y}_f = \mathbf{A}_f^o \mathbf{X}_f^o + \underline{\boldsymbol{\eta}}_f, \quad f = 1, 2, \dots, F \quad (19)$$

where  $\mathbf{A}_f^o$  are the sensing matrices;  $\underline{\boldsymbol{\eta}}_f$  are (modified) noise contributions. For brevity let us denote  $\mathbf{Y}_{1:F} \equiv \{\mathbf{Y}_1 \dots \mathbf{Y}_F\}$  and  $\mathbf{X}_{1:F}^o \equiv \{\mathbf{X}_1^o \dots \mathbf{X}_F^o\}$ . The noise  $\underline{\boldsymbol{\eta}}_f$  and the weights  $\mathbf{X}_f^o$  are assumed mutually independent and also are mutually independent across frequencies. The multi frequency likelihood then is given by

$$p(\mathbf{Y}_{1:F}|\mathbf{X}_{1:F}^o) = \prod_{f=1}^F p(\mathbf{Y}_f|\mathbf{X}_f^o) \quad (20)$$

where  $p(\mathbf{Y}_f|\mathbf{X}_f^o)$  is given by (18). We have two possibilities for the joint prior over  $\mathbf{X}_{1:F}^o$ :

*Multi-frequency-1 (MF-1):* In this model, the prior diagonal covariance matrix  $\boldsymbol{\Gamma}_f$  depends on frequency:

$$p(\mathbf{X}_f^o) = \prod_{l=1}^L \mathcal{CN}(\mathbf{x}_{f,l}^o; \mathbf{0}, \boldsymbol{\Gamma}_f), \quad f = 1, 2, \dots, F. \quad (21)$$

This model is appropriate when the variance of a source at different frequencies can be different and has been used in [38].

*Multi-frequency-2 (MF-2):* This model assumes the prior for all frequencies is governed by the same statistical distribution:

$$p(\mathbf{X}_f^o) = \prod_{l=1}^L \mathcal{CN}(\mathbf{x}_{f,l}^o; \mathbf{0}, \boldsymbol{\Gamma}), \quad f = 1, 2, \dots, F \quad (22)$$

where  $\boldsymbol{\Gamma}$  is a diagonal covariance matrix. Assuming  $\boldsymbol{\Gamma}$  is sparse, this imposes identical sparsity constraints and variances on all of the vectors  $\mathbf{X}_1^o \dots \mathbf{X}_F^o$ . This assumption of common covariance matrix has been used in [9].

## III. SPARSE BAYESIAN LEARNING

### A. Evidence

In the SBL framework [4], [6], the prior parameter  $\boldsymbol{\Gamma}$  is assumed unknown and estimated using the observed signal  $\mathbf{Y}$ . It is estimated by maximizing the evidence (also called type-II maximum likelihood). We first consider the single frequency case. The evidence  $p(\mathbf{Y})$  is obtained by averaging over all realizations of  $\mathbf{X}^o$

$$p(\mathbf{Y}) = \int p(\mathbf{Y}|\mathbf{X}^o)p(\mathbf{X}^o)d\mathbf{X}^o \quad (23)$$

$$\begin{aligned} &= \int \prod_{l=1}^L \mathcal{CN}(\mathbf{y}_l; \mathbf{A}^o \mathbf{x}_l^o, \boldsymbol{\Sigma}_{\boldsymbol{\eta}}) \mathcal{CN}(\mathbf{x}_l^o; \mathbf{0}, \boldsymbol{\Gamma}) d\mathbf{X}^o \\ &= \prod_{l=1}^L \mathcal{CN}(\mathbf{y}_l; \mathbf{0}, \boldsymbol{\Sigma}_{\boldsymbol{\eta}} + \mathbf{A}^o \boldsymbol{\Gamma} \mathbf{A}^{oH}) = \prod_{l=1}^L \mathcal{CN}(\mathbf{y}_l; \mathbf{0}, \boldsymbol{\Sigma}_{\mathbf{y}}), \end{aligned} \quad (24)$$

where  $\boldsymbol{\Sigma}_{\mathbf{y}} = \boldsymbol{\Sigma}_{\boldsymbol{\eta}} + \mathbf{A}^o \boldsymbol{\Gamma} \mathbf{A}^{oH}$ . Note that  $\boldsymbol{\Sigma}_{\mathbf{y}}$  contains both the parameters  $\sigma^2$  and  $\boldsymbol{\Gamma}$ . Ignoring the terms independent of  $\sigma^2$  and  $\boldsymbol{\Gamma}$ , the log evidence is

$$\log p(\mathbf{Y}) = \sum_{l=1}^L -\log((\pi)^N |\boldsymbol{\Sigma}_{\mathbf{y}}|) - \sum_{l=1}^L \mathbf{y}_l^H \boldsymbol{\Sigma}_{\mathbf{y}}^{-1} \mathbf{y}_l \quad (25)$$

$$\propto -L \log |\boldsymbol{\Sigma}_{\mathbf{y}}| - \text{Tr}(\mathbf{Y}^H \boldsymbol{\Sigma}_{\mathbf{y}}^{-1} \mathbf{Y}), \quad (26)$$

where  $\text{Tr}()$  denotes the trace of a matrix.

### B. Fixed point update

The estimate  $\hat{\boldsymbol{\Gamma}}$  maximizes the evidence

$$\hat{\boldsymbol{\Gamma}} = \arg \max_{\boldsymbol{\Gamma}} \log p(\mathbf{Y}) \quad (27)$$

$$= \arg \min_{\boldsymbol{\Gamma}} \left\{ L \log |\boldsymbol{\Sigma}_{\mathbf{y}}| + \text{Tr}(\mathbf{Y}^H \boldsymbol{\Sigma}_{\mathbf{y}}^{-1} \mathbf{Y}) \right\}. \quad (28)$$

One approach to solve this problem is using the EM algorithm [39] but the resulting update equations have slow convergence [4], [6]. We perform differentiation of the objective function (28) to obtain a local minima. We have the following derivative relations for  $\boldsymbol{\Sigma}_{\mathbf{y}}$

$$\frac{\partial \log |\boldsymbol{\Sigma}_{\mathbf{y}}|}{\partial \gamma_m} = \text{Tr} \left( \boldsymbol{\Sigma}_{\mathbf{y}}^{-1} \frac{\partial \boldsymbol{\Sigma}_{\mathbf{y}}}{\partial \gamma_m} \right), \quad (29)$$

$$\frac{\partial \boldsymbol{\Sigma}_{\mathbf{y}}^{-1}}{\partial \gamma_m} = -\boldsymbol{\Sigma}_{\mathbf{y}}^{-1} \frac{\partial \boldsymbol{\Sigma}_{\mathbf{y}}}{\partial \gamma_m} \boldsymbol{\Sigma}_{\mathbf{y}}^{-1}, \quad \frac{\partial \boldsymbol{\Sigma}_{\mathbf{y}}}{\partial \gamma_m} = \boldsymbol{\Sigma}_m^e + \mathbf{a}_m^o \mathbf{a}_m^{oH}. \quad (30)$$

Differentiating (28) with respect to the  $m$ th diagonal element  $\gamma_m$

$$\begin{aligned} &\frac{\partial}{\partial \gamma_m} \left\{ L \log |\boldsymbol{\Sigma}_{\mathbf{y}}| + \text{Tr}(\mathbf{Y}^H \boldsymbol{\Sigma}_{\mathbf{y}}^{-1} \mathbf{Y}) \right\} \\ &= L \text{Tr} \left( \boldsymbol{\Sigma}_{\mathbf{y}}^{-1} [\boldsymbol{\Sigma}_m^e + \mathbf{a}_m^o \mathbf{a}_m^{oH}] \right) - \\ &\quad \text{Tr} \left( \mathbf{Y}^H \boldsymbol{\Sigma}_{\mathbf{y}}^{-1} [\boldsymbol{\Sigma}_m^e + \mathbf{a}_m^o \mathbf{a}_m^{oH}] \boldsymbol{\Sigma}_{\mathbf{y}}^{-1} \mathbf{Y} \right). \end{aligned} \quad (31)$$

Equating the derivative of the objective function to zero

$$1 = \frac{1}{L} \frac{\text{Tr}(\mathbf{Y}^H \Sigma_{\mathbf{y}}^{-1} [\Sigma_m^e + \mathbf{a}_m^o \mathbf{a}_m^{oH}] \Sigma_{\mathbf{y}}^{-1} \mathbf{Y})}{\text{Tr}(\Sigma_{\mathbf{y}}^{-1} [\Sigma_m^e + \mathbf{a}_m^o \mathbf{a}_m^{oH}])} \quad (32)$$

$$\frac{\gamma_m}{\gamma_m} = \left( \frac{1}{L} \frac{\text{Tr}(\mathbf{Y}^H \Sigma_{\mathbf{y}}^{-1} [\Sigma_m^e + \mathbf{a}_m^o \mathbf{a}_m^{oH}] \Sigma_{\mathbf{y}}^{-1} \mathbf{Y})}{\text{Tr}(\Sigma_{\mathbf{y}}^{-1} [\Sigma_m^e + \mathbf{a}_m^o \mathbf{a}_m^{oH}])} \right)^b \quad (33)$$

where we introduced  $\gamma_m$  terms to obtain an iterative update equation. Since the fixed point update is not unique the exponent term  $b$  is introduced to include a broad range of update rules. Different update equations introduced in the literature can be obtained using different values of  $b$ . The update is then

$$\gamma_m^{\text{new}} \leftarrow \gamma_m^{\text{old}} \left( \frac{\text{Tr}(\Sigma_{\mathbf{y}}^{-1} [\Sigma_m^e + \mathbf{a}_m^o \mathbf{a}_m^{oH}] \Sigma_{\mathbf{y}}^{-1} \mathbf{S}_{\mathbf{y}})}{\text{Tr}(\Sigma_{\mathbf{y}}^{-1} [\Sigma_m^e + \mathbf{a}_m^o \mathbf{a}_m^{oH}])} \right)^b. \quad (34)$$

where  $\mathbf{S}_{\mathbf{y}}$  is the sample covariance matrix  $\mathbf{S}_{\mathbf{y}} = \frac{1}{L} \mathbf{Y} \mathbf{Y}^H$ . In the above update equation,  $\gamma_m^{\text{old}}$  appears explicitly as well as implicitly in the expression for  $\Sigma_{\mathbf{y}}$ .

*Remark:* There are multiple ways to formulate a fixed point update equation. Our formulation is inspired by some of the equations used in the literature [4], [6], [10] and convergence properties of the simulation results. It is not clear for what values of  $b$ , if any, convergence of (34) is guaranteed. For  $\Sigma_m^e = \mathbf{0}$  and  $\gamma^e = 0$ , a value of  $b = 1$  gives the update equation used in [4], [6] and  $b = 0.5$  gives the update equation used in [10].

### C. Multi-frequency SBL

We have two multi-frequency update rules based on the priors for  $\mathbf{X}_{1:F}$  in either (21) or (22).

1) *Multi-frequency - 1 (SBL MF-1):* With the prior (21), the likelihood (20), and the independence assumptions, the joint evidence  $p(\mathbf{Y}_{1:F})$  is

$$p(\mathbf{Y}_{1:F}) = \prod_{f=1}^F \prod_{l=1}^L \mathcal{CN}(\mathbf{y}_{f,l} | \mathbf{0}, \Sigma_{\mathbf{y}_f}). \quad (35)$$

where  $\Sigma_{\mathbf{y}_f} = \Sigma_{\eta_f} + \mathbf{A}_f^o \Gamma_f \mathbf{A}_f^{oH}$ . Since the different frequency components are decoupled, maximizing this joint evidence is the same as maximizing the evidence for each frequency individually. Thus the update rule for frequency  $f$  is

$$\gamma_{f,m}^{\text{new}} \leftarrow \gamma_{f,m}^{\text{old}} \left( \frac{\text{Tr}(\Sigma_{\mathbf{y}_f}^{-1} [\Sigma_{f,m}^e + \mathbf{a}_{f,m}^o \mathbf{a}_{f,m}^{oH}] \Sigma_{\mathbf{y}_f}^{-1} \mathbf{S}_{\mathbf{y}_f})}{\text{Tr}(\Sigma_{\mathbf{y}_f}^{-1} [\Sigma_{f,m}^e + \mathbf{a}_{f,m}^o \mathbf{a}_{f,m}^{oH}])} \right)^b. \quad (36)$$

We combine the prior covariance of individual frequencies to enforce a common sparsity profile as follows

$$\Gamma = \frac{1}{F} \sum_{f=1}^F \Gamma_f. \quad (37)$$

This multi-frequency formulation was originally derived in [38] but may be less accurate as a common sparsity profile across multiple frequencies is not fully enforced.

2) *Multi-frequency - 2 (SBL MF-2):* With the prior (22), the likelihood (20), and the independence assumptions, the joint evidence  $p(\mathbf{Y}_{1:F})$  is

$$p(\mathbf{Y}_{1:F}) = \prod_{f=1}^F p(\mathbf{Y}_f) = \prod_{f=1}^F \prod_{l=1}^L \mathcal{CN}(\mathbf{y}_{f,l} | \mathbf{0}, \Sigma_{\mathbf{y}_f}) \quad (38)$$

where  $\Sigma_{\mathbf{y}_f} = \Sigma_{\eta_f} + \mathbf{A}_f^o \Gamma \mathbf{A}_f^{oH}$ . Taking the logarithm and ignoring constant terms we have

$$\log p(\mathbf{Y}_{1:F}) \propto \sum_{f=1}^F \left( -L \log |\Sigma_{\mathbf{y}_f}| - \text{Tr}(\mathbf{Y}_f^H \Sigma_{\mathbf{y}_f}^{-1} \mathbf{Y}_f) \right). \quad (39)$$

To estimate  $\hat{\Gamma}$  we maximize the joint evidence:

$$\hat{\Gamma} = \arg \max_{\Gamma} \log p(\mathbf{Y}_{1:F}) \quad (40)$$

$$= \arg \min_{\Gamma} \left\{ \sum_{f=1}^F L \log |\Sigma_{\mathbf{y}_f}| + \text{Tr}(\mathbf{Y}_f^H \Sigma_{\mathbf{y}_f}^{-1} \mathbf{Y}_f) \right\} \quad (41)$$

To obtain a minimum of this objective function, we differentiate as before. Applying the derivative results as before and equating the derivative to zero we have

$$\frac{\partial}{\partial \gamma_m} \left\{ \sum_{f=1}^F L \log |\Sigma_{\mathbf{y}_f}| + \text{trace}(\mathbf{Y}_f^H \Sigma_{\mathbf{y}_f}^{-1} \mathbf{Y}_f) \right\} = 0 \quad (42)$$

$$\gamma_m^{\text{new}} \leftarrow \gamma_m^{\text{old}} \left( \frac{\sum_{f=1}^F \text{Tr}(\Sigma_{\mathbf{y}_f}^{-1} [\Sigma_{f,m}^e + \mathbf{a}_{f,m}^o \mathbf{a}_{f,m}^{oH}] \Sigma_{\mathbf{y}_f}^{-1} \mathbf{S}_{\mathbf{y}_f})}{\sum_{f=1}^F \text{Tr}(\Sigma_{\mathbf{y}_f}^{-1} [\Sigma_{f,m}^e + \mathbf{a}_{f,m}^o \mathbf{a}_{f,m}^{oH}])} \right)^b. \quad (43)$$

In this multi-frequency formulation, a unified update rule is obtained which combines all the frequency observations together. The single frequency update rule (34) is obtained when only one frequency is present by substituting  $F = 1$ . A similar approach of using common covariance matrix at different frequencies is adapted in [9] but the obtained multi-frequency update rule is different.

### D. Special cases

It is useful to consider some of the special cases of the generalized model in (8). Specifically we are interested in cases when either  $\mathbf{x}^e = \mathbf{0}$  or  $\mathbf{A}^e = \mathbf{0}$ . When  $\mathbf{x}^e = \mathbf{0}$  gives

$$\mathbf{y} = \mathbf{A}^o \mathbf{x}^o + \mathbf{A}^e \mathbf{x}^e + \mathbf{n} \quad (44)$$

which we refer to as SBL-1. Alternately, when  $\mathbf{A}^e = \mathbf{0}$  we get

$$\mathbf{y} = \mathbf{A}^o \mathbf{x}^o + \mathbf{A}^o \mathbf{x}^e + \mathbf{n} \quad (45)$$

which we refer to as SBL-2. When both  $\mathbf{x}^e = \mathbf{0}$  and  $\mathbf{A}^e = \mathbf{0}$  we get the regular SBL [4], [6]. Both SBL-1 and SBL-2 can be combined with the two multi-frequency formulations MF-1 and MF-2.

### E. Noise estimate

Similar to the update rule for  $\gamma_m$ , we can develop an update equation for  $\sigma^2$  by computing the derivative of the evidence with respect to  $\sigma^2$ . But the resulting update equation is not useful [6], [9], [10], possibly because of the identifiability

issue [6]. Hence we use traditional method to estimate  $\sigma^2$ . Let  $\mathbf{A}_{\mathcal{M}}$  denote the matrix formed by  $K$  columns of  $\mathbf{A}$  indexed by  $\mathcal{M}$ , where the set  $\mathcal{M}$  indicates the location of non-zero entries of  $\mathbf{x}$  with cardinality  $|\mathcal{M}| = K$ . We can estimate  $\mathcal{M}$  using  $\gamma$  through thresholding and peak picking. The noise variance estimate for frequency  $f$  is then

$$\hat{\sigma}_f^2 = \frac{1}{N-K} \text{Tr}((\mathbf{I}_N - \mathbf{A}_{f,\mathcal{M}} \mathbf{A}_{f,\mathcal{M}}^+) \mathbf{S}_{\mathbf{y}_f}), \quad (46)$$

where  $\mathbf{A}_{\mathcal{M}}^+$  denotes the Moore-Penrose pseudo-inverse of the matrix  $\mathbf{A}_{\mathcal{M}}$ . This noise estimate has been used in [9], [10], [40]. Note that the noise level at each frequency can be different whereas in [9] noise is assumed the same for all frequencies.

#### F. Posterior

Applying Bayes rule the posterior for  $\mathbf{X}$  is expressed as

$$p(\mathbf{X}|\mathbf{Y}) = \frac{p(\mathbf{Y}|\mathbf{X})p(\mathbf{X})}{p(\mathbf{Y})}. \quad (47)$$

Since the prior is a Gaussian, the likelihood is approximated to be Gaussian, and the snapshots are independent, the posterior is approximately Gaussian with density given by

$$p(\mathbf{X}|\mathbf{Y}) \approx \prod_{l=1}^L \mathcal{CN}(\mathbf{0}, \boldsymbol{\mu}_l, \boldsymbol{\Sigma}_{\mathbf{x}}), \quad (48)$$

$$\boldsymbol{\mu}_l = \boldsymbol{\Gamma} \mathbf{A}^H \boldsymbol{\Sigma}_{\mathbf{y}}^{-1} \mathbf{y}_l, \quad \forall l = 1 \dots L, \quad (49)$$

$$\boldsymbol{\Sigma}_{\mathbf{x}} = \boldsymbol{\Gamma} - \boldsymbol{\Gamma} \mathbf{A}^H \boldsymbol{\Sigma}_{\mathbf{y}}^{-1} \boldsymbol{\Gamma}. \quad (50)$$

The posterior mean  $\boldsymbol{\mu}_l$  provides an estimate of the amplitude and phase of the weight vector at the  $l$ th snapshot and also is sparse. The posterior covariance matrix  $\boldsymbol{\Sigma}_{\mathbf{x}}$  provides an estimate of uncertainty in the weights.

## IV. SIMULATIONS AND EXPERIMENTS

### A. SBL implementation

This section discusses the algorithmic implementation of the SBL update rules developed in Section III. A pseudocode of the SBL MF-2 algorithm is given in Algorithm 1. A similar algorithm can be obtained for SBL MF-1 by replacing (43) with (36)-(37). In either case, single frequency algorithm is obtained by setting  $F = 1$ . The special cases of SBL-1 and SBL-2 discussed in Section III-D are obtained by setting  $\boldsymbol{\Gamma}^e = \mathbf{0}$  and  $\boldsymbol{\Sigma}_m^e = \mathbf{0}$  respectively.

Parameters  $\epsilon$  and  $N_t$  determine the error convergence criteria and the maximum number of iterations, respectively. We set the power exponent in the update rule (43) as  $b = 1$  which empirically shows stable convergence properties. A higher value of  $b$  might lead to faster rate of convergence but could potentially suffer from poor convergence solution or oscillatory behavior.

The inputs to the algorithm are the sample covariance matrix  $\mathbf{S}_{\mathbf{y}_f}$  and the sensing matrix  $\mathbf{A}_f^o$  at the  $f$ -th frequency, and *tuning* parameters  $\gamma_m^e$  and  $\boldsymbol{\Sigma}_m^e$ . When  $F$  frequencies are present,  $f$  takes values in the range  $f = 1, 2, \dots, F$ . The parameters to estimate,  $\gamma_m$  and  $\sigma_f^2$ , are initialized to constant non-zero values. The parameter  $\gamma_m$  can be frequency dependent, see

Section III-C, in which case there is an additional loop over the frequency variable (not shown here). The  $\gamma_m$  variables are updated using the update rule (43). Appropriate number ( $K$ ) of peaks and their locations are identified from current estimate of  $\gamma$  and used to construct  $\mathbf{A}_{\mathcal{M}}$ . Then the frequency dependent noise estimate is obtained from (46). Though we assume  $K$  to be known for estimating  $\hat{\sigma}^2$ , this can be avoided by using model order identification methods [9] to first estimate  $\hat{K}$  and then estimate  $\hat{\sigma}^2$ .

---

### Algorithm 1 Multi frequency SBL algorithm

---

```

1: Parameters:  $\epsilon = 10^{-6}$ ,  $N_t = 3000$ ,  $b = 1$ 
2: Input:  $\mathbf{S}_{\mathbf{y}_f}$ ,  $\mathbf{A}_f^o \forall f$ ,  $\gamma_m^e$ ,  $\boldsymbol{\Sigma}_m^e \forall m$ 
3: Initialization:  $\gamma_m^{\text{old}} = 1$ ,  $\forall m$ ,  $\hat{\sigma}_f^2 = 0.1$ ,  $\forall f$ 
4: for  $i \leftarrow 1, N_t$  do
5:   Compute:  $\boldsymbol{\Sigma}_{\mathbf{y}_f} = \hat{\sigma}_f^2 \mathbf{I} + \mathbf{A}_f^o \boldsymbol{\Gamma}^{\text{old}} \mathbf{A}_f^{oH} \forall f$ .
6:    $\gamma_m$  update  $\forall m$  using (43)
7:    $\hat{\sigma}_f^2$  estimate  $\forall f$  using (46)
8:   If  $\frac{\|\gamma_m^{\text{new}} - \gamma_m^{\text{old}}\|_1}{\|\gamma_m^{\text{old}}\|_1} < \epsilon$ , break
9:    $\gamma_m^{\text{old}} = \gamma_m^{\text{new}} \forall m$ 
10:  end for

```

---

We consider the two models discussed as special cases in Section III-D. SBL-1 is obtained by setting  $\gamma_m^e = 0$  and SBL-2 is obtained by setting  $\boldsymbol{\Sigma}_m^e = \mathbf{0}$  for all  $m$ . When both  $\gamma_m^e = 0$  and  $\boldsymbol{\Sigma}_m^e = \mathbf{0}$  we get the original SBL which we refer to as simply SBL. Additionally we make the following assumption in our implementation

$$\boldsymbol{\Sigma}_m^e = \phi^e \mathbf{I}_N, \quad \forall m \quad (51)$$

$$\gamma_m^e = \gamma^e, \quad \forall m. \quad (52)$$

This simplifies the number of free tuning parameters in our algorithm and allows for a systematic study of them. The use of constant values  $\phi^e$  and  $\gamma^e$  is justified when all the mismatch and errors are expected to have similar statistics. The actual values of  $\phi^e$  and  $\gamma^e$  ideally would depend on the SNR and application of interest. In this paper, we first explore a range of tuning parameter values and keep the ones which give the ‘best’ performance.

### B. Beamforming

We use beamforming simulations to demonstrate the proposed SBL algorithms. In plane wave beamforming, the observed signal model is a linear combination of plane waves from different angles. Since the number of sources (arrival angles) is small, finely dividing the angle space results in a vector  $\mathbf{x}$  of complex amplitudes which is sparse. SBL is used to recover the arrival angles of the plane waves and their complex amplitudes.

For a narrow band signal of wavelength  $\lambda$  and uniform sensor array separation of  $d$ , the sensing matrix columns for beamforming are

$$\mathbf{a}_m^o = \frac{1}{\sqrt{N}} [1, e^{-j2\pi \frac{d}{\lambda} \sin(\theta_m)}, \dots, e^{-j2\pi \frac{(N-1)d}{\lambda} \sin(\theta_m)}]^T \quad (53)$$

for  $m = 1 \dots M$  where  $\theta_m$  is the  $m$ th discretized angle. The angle space  $[-90, 90]^\circ$  is discretized with  $1^\circ$  separation giving  $M = 181$ . We consider  $N = 20$  sensors.

We consider a beamforming problem with three sources located at angles  $[-20, -15, 75]^\circ$  with power  $[10, 22, 20]$  dB respectively. The phase of each source is assumed to be uniformly random in each snapshot. Though in Section II-A the source amplitudes are assumed to be random with complex Gaussian density, in simulations only the phases are assumed random and the magnitudes are constant. In this section we assume single frequency analysis with a sensor separation of  $d = \frac{\lambda}{2}$ .  $L = 30$  snapshots are processed.

A comparison of the different processing methods is provided in Figure 1. The SBL method is compared with traditional DoA estimation methods such as conventional beamformer (CBF), minimum variance distortionless response (MVDR), and MUSIC. For a brief review of these methods see [10]. The average root mean square error (RMSE) and SNR are computed as

$$\text{Avg. RMSE} = E \left\{ \sqrt{\frac{1}{K} \sum_{k=1}^K (\hat{\theta}_k - \theta_k)^2} \right\} \quad (54)$$

$$\text{SNR}_f = 10 \log \frac{E\{\|\mathbf{x}_f^o\|_2^2\}}{\sigma_f^2} \quad (55)$$

where  $\theta_k$  are the true source angles and  $\hat{\theta}_k$  are the estimated source angles. The expectation in Avg. RMSE is computed from multiple Monte Carlo runs of the simulation. For SNR computation, since source amplitudes are fixed in the simulations,  $E\{\|\mathbf{x}_f^o\|_2^2\} = \|\mathbf{x}_f^o\|_2^2$ . For traditional DoA methods, the estimated source angles are chosen to be the top  $K$  peak locations in the angular power spectrum while for SBL they are chosen to be the top  $K$  peak locations of  $\gamma$ .

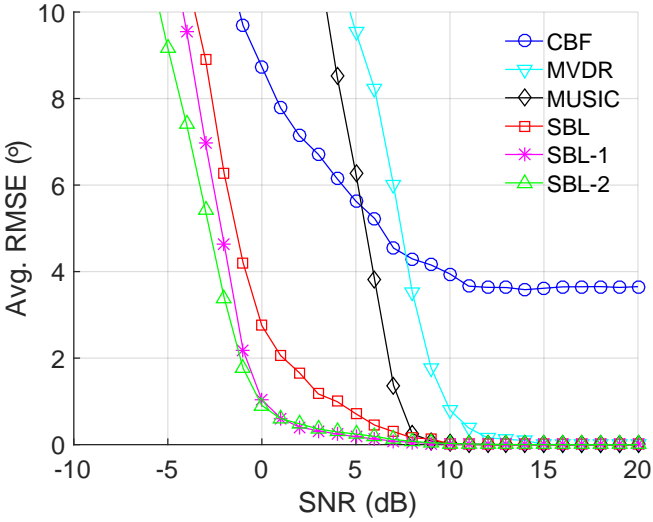


Fig. 1: Comparison of DoA estimation methods: CBF, MVDR, MUSIC, SBL, SBL-1, SBL-2 using 500 random trials.

Figure 1 also compares SBL-1 and SBL-2 algorithms with parameters  $\phi^e = 0.03$  and  $\gamma^e = 1.2$  respectively. We observe that SBL-1 and SBL-2 show slightly reduced Avg. RMSE than SBL at low SNR indicating improved DOA estimation ability

even though there is no perturbation in  $\mathbf{A}$  or  $\mathbf{x}$  (i.e.  $\mathbf{A}^e = \mathbf{0}$  and  $\mathbf{x}^e = \mathbf{0}$ ). SBL outperforms the other methods of CBF, MVDR and MUSIC. The performance of these algorithms for a range of  $\phi^e$  and  $\gamma^e$  is shown in Figure 2. Specifically for SBL-1,  $\phi^e \in [0, 0.05]$  and for SBL-2,  $\gamma^e \in [0, 2]$ . As the value of  $\phi^e$  and  $\gamma^e$  is increased the performance of SBL first improves and later starts to degrade. The lowest error is roughly achieved when  $\phi^e = 0.03$  and  $\gamma^e = 1.2$ .

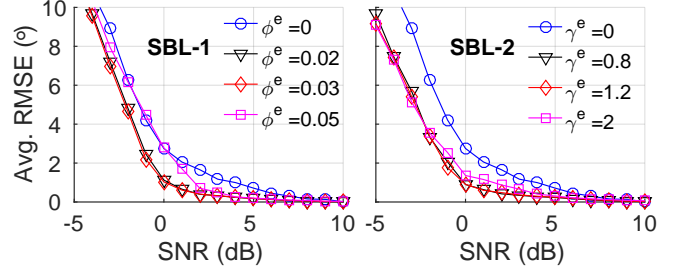


Fig. 2: Effect of tuning parameters  $\phi^e$  and  $\gamma^e$  on DoA estimation for SBL-1 and SBL-2 respectively.

Figure 3 demonstrates the power spectrum for different methods. For conventional beamformer (CBF) the power spectrum is  $P(\theta_m) = \mathbf{a}_m^{oH} \mathbf{S}_y \mathbf{a}_m^o$ . For SBL based methods,  $\gamma$  at convergence is treated as power spectrum as it corresponds to prior variance of the zero mean source. The SNR (55) is  $-3$  dB. From Figure 3 the CBF has very broad peaks and the weaker peak at  $-20^\circ$  is poorly identified. The SBL power spectrums are clearly sparse in comparison to CBF.

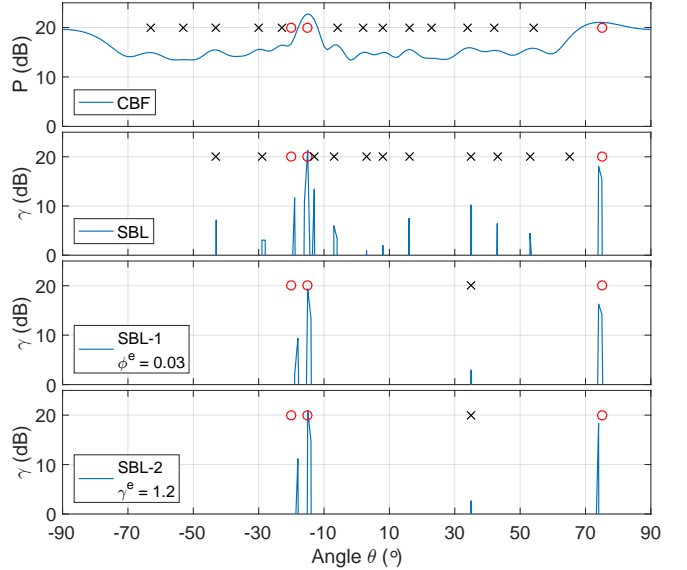


Fig. 3: Power spectrum of CBF and  $\gamma$  of SBL when three sources are present at  $[-20, -15, 75]^\circ$  with power  $[10, 22, 20]$  dB. Red circles correspond to true peak locations and black cross markers correspond to false peaks.

In regular SBL, many false/spurious peaks also are present since the SNR is low. The strongest peak is split into two peaks as seen in Figure 3. These false/spurious peaks compete with the weaker peak and represent errors in  $\mathbf{x}$ . Modifications

to the SBL i.e. SBL-1 ( $\phi^e = 0.03$ ) and SBL-2 ( $\gamma^e = 1.2$ ) result in improved performance. The number of false peaks are considerably reduced and there is no splitting of the strongest peak. The SBL-1 has a drawback in that along with reduced false peaks, it reduces the magnitude of the true peaks. This effect is smaller with SBL-2. The modified SBL algorithms work better than performing a thresholding operation on SBL. The spurious peaks are suppressed significantly without compromising on the strength of the weaker peak at  $-20^\circ$ .

### C. Multi-frequency analysis

Significant performance gain can be obtained by processing multiple frequencies simultaneously. We consider the beamforming example from previous section with three sources located at angles  $[-20, -15, 75]^\circ$  and power  $[10, 22, 20]$  dB respectively,  $L = 30$ . The algorithm SBL-2 MF-2 is used in the simulations. In multi-frequency simulations, same source power is simulated at all the frequencies which is the assumption of MF-2 formulation.

The multi-frequency gain can be seen from single and multi-frequency RMSE versus SNR plots in Figure 4. The frequencies for  $F = 1, 2, 4$  are  $\{F_0\}$ ,  $\{F_0, 2F_0\}$ , and  $\{F_0, 2F_0, 3F_0, 4F_0\}$  respectively. To avoid aliasing effects, as the number of frequencies is increased, a sensor separation of  $d = \frac{\lambda_{\min}}{2}$  is maintained where  $\lambda_{\min}$  is the smallest wavelength when processing multi-frequency data. Since the number of sensors is kept constant at  $N = 20$ , the relative aperture sizes are in the ratio  $4 : 2 : 1$ . We observe that as more frequencies are used there is reduction in angle localization error for regular SBL ( $\gamma^e = 0$ ). Additionally, using the SBL-2 with  $\gamma^e = 0.8$  further reduces the RMSE.

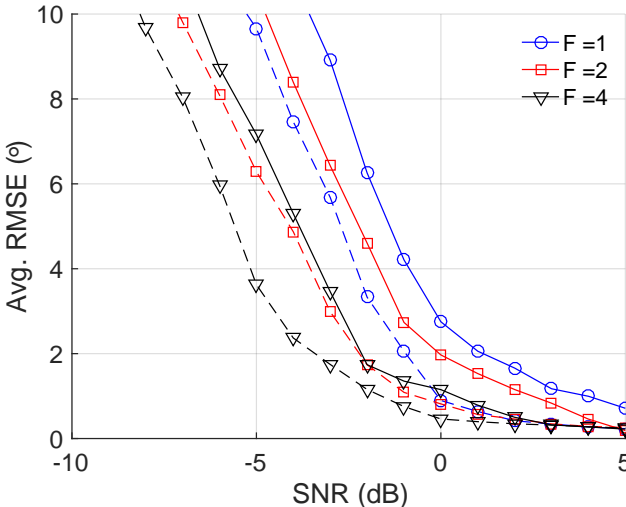


Fig. 4: SBL-2 MF-2: Multi frequency analysis with  $\gamma^e = 0$  (solid) and  $\gamma^e = 0.8$  (dashed) with constant number of sensors  $N = 20$  as number of frequencies increased from  $F = 1$  to  $F = 4$ .

### D. Effect of aliasing on SBL

An interesting analysis of SBL is possible while processing multiple frequencies and some or all of which experience

aliasing. A discussion on aliasing suppression for wide band signals using compressive processing is provided in [41]. A large array aperture and hence a large sensor array spacing is desirable to obtain higher resolution. A drawback of large array spacing is that it limits the highest frequency that can be processed without encountering aliasing<sup>1</sup>. This drawback partially can be overcome by multi frequency SBL. Based on the first formulation in Section III-C, a common sparsity profile is imposed on all the frequencies. Since the aliasing location differs for each frequency, the aliased peaks are suppressed by jointly processing multi-frequency observations.

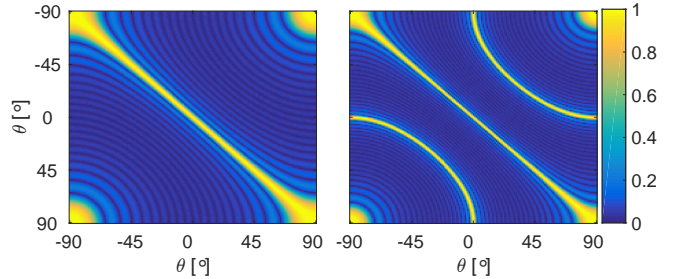


Fig. 5: Gram matrices for two array spacings :  $d = \frac{\lambda}{2}$  (left),  $d = \lambda$  (right). Number of sensors  $N = 20$ .

The Gram matrix ( $\mathbf{A}^H \mathbf{A}$ ) for two array spacings are shown in Figure 5,  $N = 20$ . For a ULA spacing of  $d = \frac{\lambda}{2}$  there is one main lobe for each angle. When the spacing is doubled, i.e.  $d = \lambda$ , grating (side) lobes of significant strength appear which cause aliasing.

SBL (and its proposed variants SBL-1 and SBL-2) cannot avoid aliasing when a single frequency is present. Let  $f_1$  and  $f_2 = 2f_1$  be two frequencies of interest with wavelengths  $\lambda_1$  and  $\lambda_2$ . Figure 6a shows effect of aliasing when each of these frequencies are processed independently. Histogram of top three peak locations obtained from  $\gamma$  are plotted. True source locations indicated by red circles. Aliasing is absent in Figure 6a (top) as sensor spacing is half a wavelength. Doubling the signal frequency with the same sensor spacing (bottom), gives aliased peaks (location of aliased peak is indicated by black cross markers). Higher frequency gives higher resolution but at the cost of additional aliased peaks.

Processing frequencies  $f_1$  and  $f_2$  simultaneously using SBL MF-2 gives histograms of the top three peaks as shown in Figure 6b. In top plot there is no aliasing present as sensor spacing is half of the smallest wavelength. Doubling the sensor spacing increase the aperture and resolution but introduce aliasing for frequency  $f_2$ . Since SBL enforces common sparsity across the frequencies the aliased peaks are suppressed, Figure 6b (bottom).

This behavior of SBL in presence of aliasing is qualified in the RMSE vs SNR plots in Figure 7. Three curves are shown corresponding to single frequency ( $f_1$ ) without aliasing, two frequencies ( $f_1$  and  $f_2$ ) without aliasing, and two frequencies ( $f_1$  and  $f_2$ ) with one frequency ( $f_2$ ) aliased. The error is lower

<sup>1</sup>This is true for uniform linear arrays. The preferred setup is a random array which has low coherence between weight vectors [12]. For random arrays there is no aliasing.

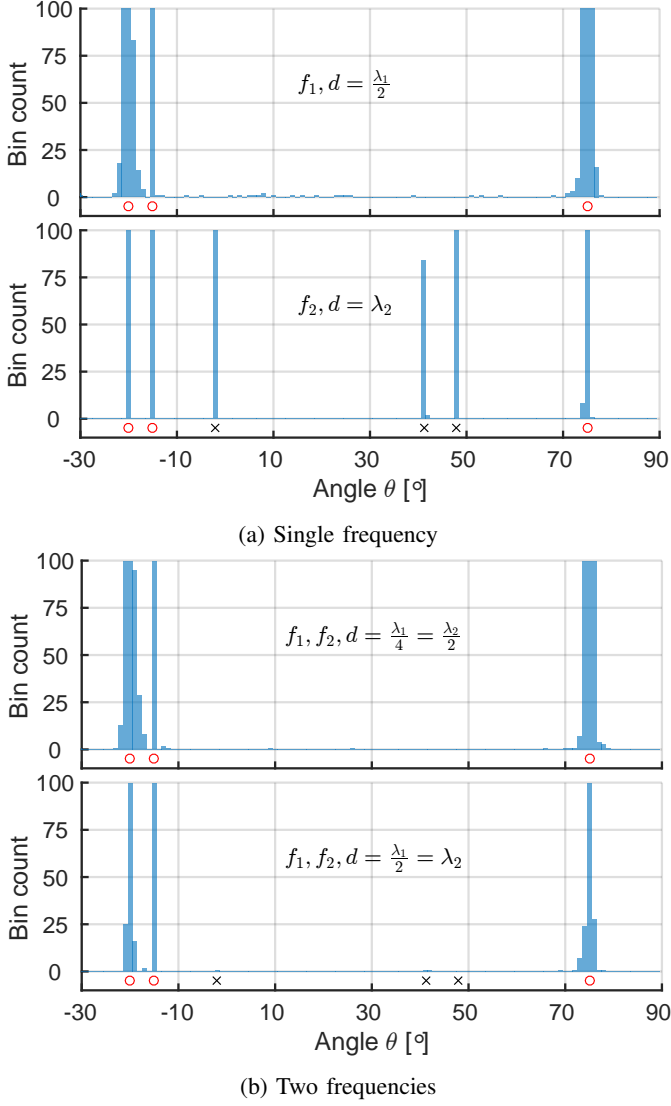


Fig. 6: Aliasing analysis using histogram of top three peaks: (a) Single frequency - half wavelength spacing (top) and full wavelength spacing (bottom). (b) Two frequencies - no aliasing (top) and aliasing present in one frequency (bottom). Number of sensors  $N = 20$ .

in presence of aliasing because of improved resolution (due to larger aperture) and aliasing suppression by multi-frequency SBL processing. The error is further reduced by using SBL-2 analysis with  $\gamma^e = 1.2$ .

#### E. Real data analysis

The high-resolution performance of SBL is compared with CBF and is validated with experimental data in a complex multi-path, shallow-water environment.

The data set is taken from the shallow water evaluation cell experiment 1996 (SWellEx-96) Event S5 [14] collected on a 64-element vertical linear array. Element 43 is excluded from processing. The array has uniform inter-sensor spacing of 1.875 m and spans the lower part of the 212 m watercolumn from 94 to 212 m. During the 77 min Event S5, two sources,

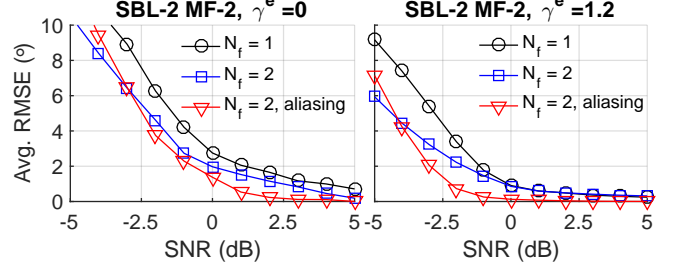


Fig. 7: RMSE vs SNR while processing a different number of frequencies - single frequency without aliasing ( $N_f = 1$ ), two frequencies without aliasing ( $N_f = 2$ ), two frequencies with one aliased ( $N_f = 2$ , aliased).

a shallow and a deep, were towed simultaneously from 9 km southwest to 3 km northeast of the array at a speed of 5 kn (2.5 m/s). The vicinity of the closest point of approach (CPA), 900 m from the array, occurred around 60 min into the event.

Each source was transmitting a unique set of tones, ranging from 49 Hz to 388 Hz. Here, we are interested in the deep source towed at approximately 60 m depth. The deep source submitted a set of three frequencies [166,283,388] Hz used for processing, with source levels at approximately 158 dB re  $1\mu$  Pa. The data are split into 2257 partially overlapping segments, whereas a single segment is of 2.7 s duration. Snapshots are computed continuously from the data before being designated to a segment. A FFT length of 2048 samples (1.35 s) with 50% overlap results in  $L = 3$  snapshots for each segment with a FFT bin width of 0.75 Hz. For this high SNR data set, our algorithm searches the adjacent  $\pm 1$  FFT bins and extracts the FFT value corresponding to the maximum bin power to accommodate Doppler shift.

Both the full array (63 elements) and a subset (21 elements) are used for processing. We refer to the full array and its subset as Array-1 and Array-2 respectively. The Array-2 is obtained by including every third element from Array-1 (Array-1 spacing  $\frac{d}{2}$  and Array-2 spacing  $\frac{3d}{2}$ ). By design, Array-1 suffers no aliasing in the frequency range of interest whereas Array-2 suffers aliasing for frequencies above 133 Hz.

Single frequency (388 Hz) data is processed using both Array-1 and Array-2. Figure 8a shows CBF output power and  $\gamma$  for SBL as the source moves over time. Array-1 processing does not suffer from aliasing (Figure 8a, left) and multi path arrivals can be seen. SBL provides finer angular resolution than CBF. Significant aliasing (Figure 8a, right) is present in both the SBL and CBF outputs when Array-2 is used. This aliasing is because of insufficient spacial sampling. Significant energy is redistributed into aliased locations.

Combining three frequencies (166, 283, and 388 Hz) and processing them using Array-1 and Array-2 is shown in Figure 8b. The SBL MF-2 is used which imposes identical sparsity constraints at all frequencies. Neither SBL nor CBF show aliasing when Array-1 (Figure 8b, left) data is processed. For Array-2 (Figure 8b, right), CBF exhibits aliasing since the surfaces are averaged across frequencies. The relatively steep true arrivals around  $\pm 20^\circ$  can easily get masked by the aliased

arrivals causing DoA estimation errors. SBL shows no aliasing with Array-2 as the multi-frequency data is (semi-)coherently processed enforcing common sparsity across frequencies. The multi path structure is preserved but in general there are slightly fewer peaks identified when processing Array-2 because of the reduced array gain.

## V. CONCLUSIONS

In this paper, we study the sparse Bayesian learning algorithm for compressed sensing and propose improvements and extensions of it. Specifically, we modified the signal model to include errors in the sensing matrix and weights as part of the linear signal model. The resulting non-Gaussian model was approximated as Gaussian by computing the first and second order statistics and the modified SBL update rule was developed. Extensions of SBL to process multiple frequencies also are proposed. Simulations and real data are used to demonstrate the advantage of multi-frequency SBL to obtain processing gain and to avoid aliasing.

## APPENDIX A COMPLEX GAUSSIAN

In this paper we only consider circularly symmetric complex Gaussian densities. The mean is assumed to be non-zero in general hence the point of circular symmetry is the mean instead of the origin. If a  $k$  dimensional complex valued random vector  $\mathbf{x}$  has a circularly symmetric complex Gaussian density given by  $\mathcal{CN}(\mathbf{x}; \boldsymbol{\mu}, \boldsymbol{\Sigma})$  then its density is given by

$$p(\mathbf{x}) = \frac{1}{\pi^k \det(\boldsymbol{\Sigma})} \exp\left(-(\mathbf{x} - \boldsymbol{\mu})^H \boldsymbol{\Sigma}^{-1} (\mathbf{x} - \boldsymbol{\mu})\right) \quad (56)$$

where  $\boldsymbol{\Sigma}$  is a Hermitian and non-negative definite matrix. From circular symmetry

$$\mathbb{E}[(\mathbf{x} - \boldsymbol{\mu})(\mathbf{x} - \boldsymbol{\mu})^H] = \boldsymbol{\Sigma} \quad (57)$$

$$\mathbb{E}[(\mathbf{x} - \boldsymbol{\mu})(\mathbf{x} - \boldsymbol{\mu})^T] = \mathbf{0}. \quad (58)$$

## APPENDIX B GAUSSIAN IDENTITIES

Let  $\mathbf{x} \in \mathbb{C}^M$  and  $\mathbf{y} \in \mathbb{C}^N$  be circularly symmetric complex Gaussian random vectors and let  $\mathbf{A} \in \mathbb{C}^{N \times M}$  be a deterministic matrix. A product relation for Gaussian densities [] is

$$\begin{aligned} \mathcal{CN}(\mathbf{x}; \boldsymbol{\mu}, \boldsymbol{\Sigma}_x) \times \mathcal{CN}(\mathbf{y}; \mathbf{Ax}, \boldsymbol{\Sigma}_y) \\ = \mathcal{CN}(\mathbf{x}; \tilde{\boldsymbol{\mu}}, \tilde{\boldsymbol{\Sigma}}_x) \times \mathcal{CN}(\mathbf{y}; \mathbf{A}\boldsymbol{\mu}, \boldsymbol{\Sigma}_y + \mathbf{A}\boldsymbol{\Sigma}_x\mathbf{A}^H) \end{aligned} \quad (59)$$

$$\tilde{\boldsymbol{\mu}} = \boldsymbol{\mu} + \mathbf{K}(\mathbf{y} - \mathbf{A}\boldsymbol{\mu}), \quad \tilde{\boldsymbol{\Sigma}}_x = (\mathbf{I} - \mathbf{KA})\boldsymbol{\Sigma}_x \quad (60)$$

$$\mathbf{K} = \boldsymbol{\Sigma}_x \mathbf{A}^H (\boldsymbol{\Sigma}_y + \mathbf{A}\boldsymbol{\Sigma}_x\mathbf{A}^H)^{-1}. \quad (61)$$

Integrating the above with respect to  $\mathbf{x}$  we get the identity

$$\begin{aligned} \int \mathcal{CN}(\mathbf{x}; \boldsymbol{\mu}, \boldsymbol{\Sigma}_x) \mathcal{CN}(\mathbf{y}; \mathbf{Ax}, \boldsymbol{\Sigma}_y) d\mathbf{x} \\ = \mathcal{CN}(\mathbf{y}; \mathbf{A}\boldsymbol{\mu}, \boldsymbol{\Sigma}_y + \mathbf{A}\boldsymbol{\Sigma}_x\mathbf{A}^H). \end{aligned} \quad (62)$$

## APPENDIX C MULTIPLICATIVE NOISE

Perturbations in the sensing matrix can arise from multiplicative noise [42]–[44]

$$\mathbf{A} = \mathbf{A}^o \circ \mathbf{A}^e \quad (63)$$

where  $\mathbf{A}^o$  is a deterministic matrix, and  $\mathbf{A}^e$  represents the multiplicative error in  $\mathbf{A}$ . The notation  $\circ$  denotes the Schur-Hadamard product of two matrices of same dimensions, i.e. the element-wise product of matrices given by

$$[\mathbf{A}^o \circ \mathbf{A}^e]_{ij} = [\mathbf{A}^o]_{ij} [\mathbf{A}^e]_{ij} \quad (64)$$

A first order expansion of the above multiplicative model can be written as

$$\mathbf{A} \approx \mathbf{A}^o \circ (\mathbf{1}_N + \mathbf{A}^{e_1}) \quad (65)$$

$$= \mathbf{A}^o + \mathbf{A}^o \circ \mathbf{A}^{e_1} \quad (66)$$

$$= \mathbf{A}^o + \mathbf{A}^{e_2}. \quad (67)$$

where  $\mathbf{A}^{e_2} = \mathbf{A}^o \circ \mathbf{A}^{e_1}$ . The model in (66) has been studied in [42]–[44] and the model in (67) has been studied in [27]–[30], [45], [46].

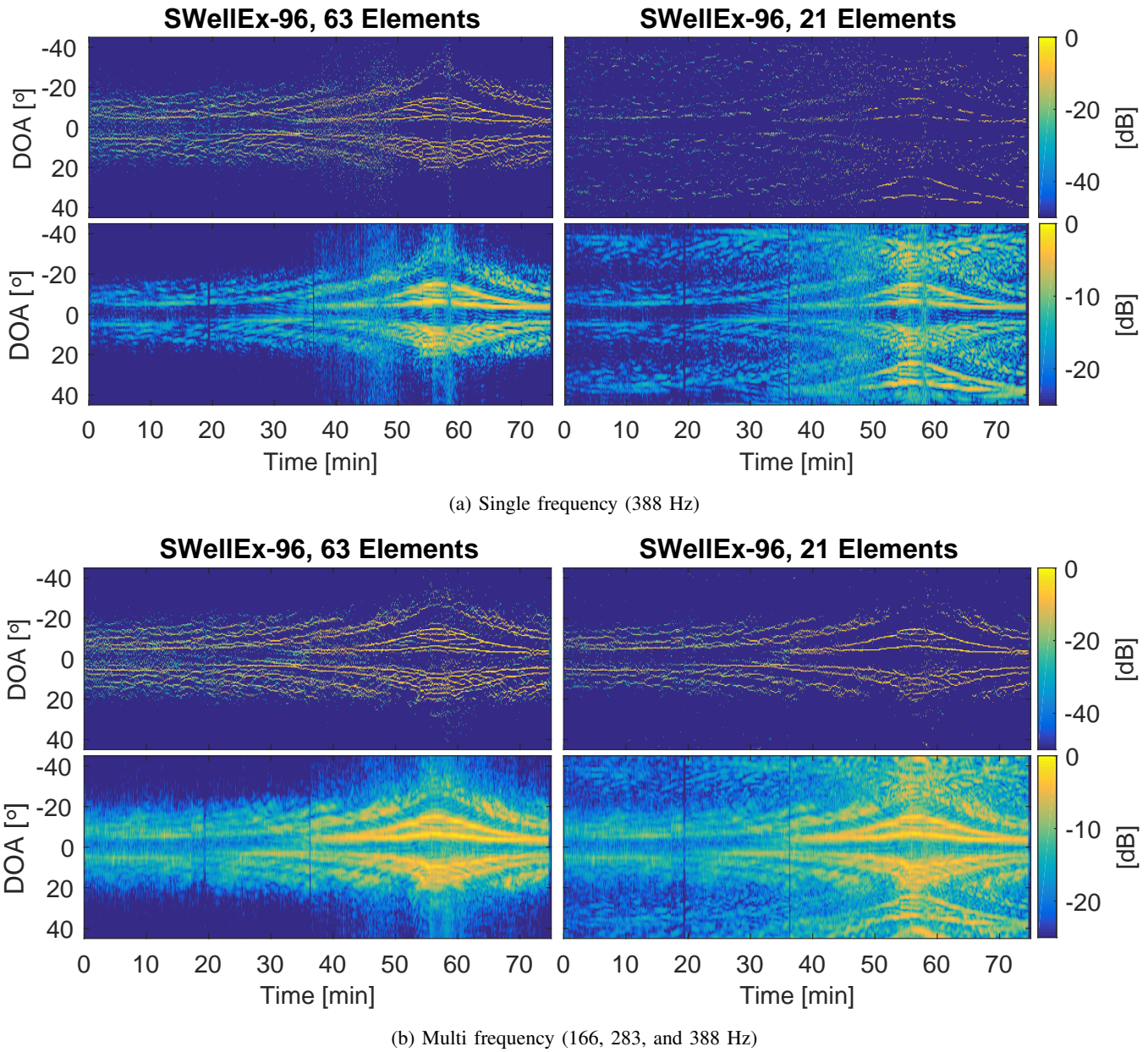


Fig. 8: (a) Single frequency (388 Hz) and (b) Multi frequency (166, 283, and 388 Hz) analysis of SwellEx-96 Event S5 data using 63 and 21 elements of the array. The top row is SBL MF-2 and bottom row is CBF.

## REFERENCES

- [1] S. S. Chen, D. L. Donoho, and M. A. Saunders, "Atomic decomposition by basis pursuit," *SIAM review*, vol. 43, no. 1, pp. 129–159, 2001.
- [2] R. Tibshirani, "Regression shrinkage and selection via the lasso," *J. Royal Stat. Soc. Series B (Methodological)*, vol. 58, no. 1, pp. 267–288, 1996.
- [3] S. G. Mallat and Z. Zhang, "Matching pursuits with time-frequency dictionaries," *IEEE Trans. Sig. Proc.*, vol. 41, no. 12, pp. 3397–3415, 1993.
- [4] M. E. Tipping, "Sparse Bayesian learning and the relevance vector machine," *J. Machine Learning Research*, vol. 1, pp. 211–244, Jun. 2001.
- [5] D. P. Wipf and B. D. Rao, "Sparse Bayesian learning for basis selection," *IEEE Trans. Sig. Proc.*, vol. 52, no. 8, pp. 2153–2164, 2004.
- [6] ———, "An empirical Bayesian strategy for solving the simultaneous sparse approximation problem," *IEEE Trans. Sig. Proc.*, vol. 55, no. 7, pp. 3704–3716, Jul. 2007.
- [7] S. Ji, Y. Xue, and L. Carin, "Bayesian compressive sensing," *IEEE Trans. Sig. Proc.*, vol. 56, no. 6, pp. 2346–2356, Jun. 2008.
- [8] Z. Zhang and B. D. Rao, "Sparse signal recovery with temporally correlated source vectors using sparse Bayesian learning," *IEEE J. Sel. Topics Sig. Proc.*, vol. 5, no. 5, pp. 912–926, 2011.
- [9] Z.-M. Liu, Z.-T. Huang, and Y.-Y. Zhou, "An efficient maximum likelihood method for direction-of-arrival estimation via sparse Bayesian learning," *IEEE Trans. Wireless Comm.*, vol. 11, no. 10, pp. 1–11, 2012.
- [10] P. Gerstoft, C. F. Mecklenbräuker, A. Xenaki, and S. Nannuru, "Multi snapshot sparse Bayesian learning for DOA," *IEEE Sig. Proc. Letters*, vol. 23, no. 10, pp. 1469–1473, Oct. 2016.
- [11] D. Malioutov, M. Çetin, and A. S. Willsky, "A sparse signal reconstruction perspective for source localization with sensor arrays," *IEEE Trans. Sig. Proc.*, vol. 53, no. 8, pp. 3010–3022, 2005.
- [12] A. Xenaki, P. Gerstoft, and K. Mosegaard, "Compressive beamforming," *J. Acoust. Soc. Am.*, vol. 136, no. 1, pp. 260–271, 2014.
- [13] P. A. Forero and P. A. Baxley, "Shallow-water sparsity-cognizant source-location mapping," *J. Acoust. Soc. Am.*, vol. 135, no. 6, pp. 3483–3501, 2014.
- [14] K. L. Gemba, W. S. Hodgkiss, and P. Gerstoft, "Adaptive and compressive matched field processing," *J. Acoust. Soc. Am.*, vol. 141, no. 1, 2017.
- [15] D. P. Wipf and S. S. Nagarajan, "A new view of automatic relevance determination," in *Adv. Neural Inf. Proc. Sys.*, vol. 20, 2008, pp. 1625–1632.
- [16] D. Wipf and S. Nagarajan, "Iterative reweighted L1 and L2 methods for finding sparse solutions," *IEEE J. Selected Topics Sig. Proc.*, vol. 4, no. 2, pp. 317–329, Apr. 2010.
- [17] P. Pal and P. P. Vaidyanathan, "Parameter identifiability in sparse Bayesian learning," in *IEEE Intl. Conf. Acoustics, Speech, Sig. Proc.*, Florence, Italy, May 2014, pp. 1851–1855.
- [18] R. Prasad and C. R. Murthy, "Cramér-Rao-type bounds for sparse Bayesian learning," *IEEE Trans. Sig. Proc.*, vol. 61, no. 3, pp. 622–632, Feb. 2013.
- [19] R. Giri and B. Rao, "Type I and type II Bayesian methods for sparse signal recovery using scale mixtures," *IEEE Trans. Sig. Proc.*, vol. 64, no. 13, pp. 3418–3428, Jul. 2016.
- [20] S. Rangan, "Generalized approximate message passing for estimation with random linear mixing," in *IEEE Intl. Sym. Inf. Theory Proceedings*, Jul. 2011.
- [21] J. P. Vila and P. Schniter, "Expectation-maximization Gaussian-mixture approximate message passing," *IEEE Trans. Sig. Proc.*, vol. 61, no. 19, pp. 4658–4672, Oct. 2013.
- [22] P. Gerstoft, A. Xenaki, and C. F. Mecklenbräuker, "Multiple and single snapshot compressive beamforming," *J. Acoust. Soc. Am.*, vol. 138, no. 4, pp. 2003–2014, 2015.
- [23] H. Cox, R. Zeskind, and M. Owen, "Robust adaptive beamforming," *IEEE Trans. Acoustics, Speech, Sig. Proc.*, vol. 35, no. 10, pp. 1365–1376, 1987.
- [24] S. A. Vorobyov, A. B. Gershman, and Z.-Q. Luo, "Robust adaptive beamforming using worst-case performance optimization: A solution to the signal mismatch problem," *IEEE Trans. Sig. Proc.*, vol. 51, no. 2, pp. 313–324, 2003.
- [25] S. Shahbazpanahi, A. B. Gershman, Z.-Q. Luo, and K. M. Wong, "Robust adaptive beamforming for general-rank signal models," *IEEE Trans. Sig. Proc.*, vol. 51, no. 9, pp. 2257–2269, Sep. 2003.
- [26] R. G. Lorenz and S. P. Boyd, "Robust minimum variance beamforming," *IEEE Trans. Sig. Proc.*, vol. 53, no. 5, pp. 1684–1696, 2005.
- [27] W. Zhang and S. A. Vorobyov, "Joint robust transmit/receive adaptive beamforming for MIMO radar using probability-constrained optimization," *IEEE Sig. Proc. Letters*, vol. 23, no. 1, pp. 112–116, Jan. 2016.
- [28] M. A. Herman and T. Strohmer, "General deviants: An analysis of perturbations in compressed sensing," *IEEE J. Sel. Topics Sig. Proc.*, vol. 4, no. 2, pp. 342–349, Apr. 2010.
- [29] H. Zhu, G. Leus, and G. B. Giannakis, "Sparsity-cognizant total least-squares for perturbed compressive sampling," *IEEE Trans. Sig. Proc.*, vol. 59, no. 5, pp. 2002–2016, May 2011.
- [30] O. Teke, A. C. Gurbuz, and O. Arikan, "Perturbed orthogonal matching pursuit," *IEEE Trans. Sig. Proc.*, vol. 61, no. 24, pp. 6220–6231, Dec. 2013.
- [31] J. T. Parker, V. Cevher, and P. Schniter, "Compressive sensing under matrix uncertainties: An approximate message passing approach," in *45th Asilomar Conf. Sig., Sys., Comp.*, Pacific Grove, CA, U.S.A., Nov. 2011.
- [32] Z. M. Liu and Y. Y. Zhou, "A unified framework and sparse Bayesian perspective for direction-of-arrival estimation in the presence of array imperfections," *IEEE Trans. Sig. Proc.*, vol. 61, no. 15, pp. 3786–3798, Aug. 2013.
- [33] X. Wu, W. P. Zhu, and J. Yan, "Direction of arrival estimation for off-grid signals based on sparse Bayesian learning," *IEEE J. Sensors*, vol. 16, no. 7, pp. 2004–2016, Apr. 2016.
- [34] I. Fedorov, R. Giri, B. D. Rao, and T. Q. Nguyen, "Robust Bayesian method for simultaneous block sparse signal recovery with applications to face recognition," in *IEEE Intl. Conf. Image Proc.*, Phoenix, Arizona, USA, Sep. 2016.
- [35] A. L. Swindlehurst and T. Kailath, "A performance analysis of subspace-based methods in the presence of model errors. I. The MUSIC algorithm," *IEEE Trans. Sig. Proc.*, vol. 40, no. 7, pp. 1758–1774, Jul. 1992.
- [36] F. Chapeau-Blondeau and D. Rousseau, "Noise-enhanced performance for an optimal Bayesian estimator," *IEEE Trans. Sig. Proc.*, vol. 52, no. 5, pp. 1327–1334, May 2004.
- [37] H. Chen, P. K. Varshney, S. M. Kay, and J. H. Michels, "Theory of the stochastic resonance effect in signal detection: Part I - fixed detectors," *IEEE Trans. Sig. Proc.*, vol. 55, no. 7, pp. 3172–3184, Jul. 2007.
- [38] P. Gerstoft and C. F. Mecklenbräuker, "Wideband sparse Bayesian learning for DOA estimation from multiple snapshots," in *IEEE Sensor Array and Multichannel Sig. Proc. Workshop*, Rio de Janeiro, Brazil, Jul. 2016.
- [39] A. P. Dempster, N. M. Laird, and D. B. Rubin, "Maximum likelihood from incomplete data via the EM algorithm," *J. Royal Stat. Soc. Series B (Methodological)*, pp. 1–38, 1977.
- [40] P. Stoica and A. Nehorai, "On the concentrated stochastic likelihood function in array signal processing," *Circuits, Sys., Sig. Proc.*, vol. 14, no. 5, pp. 669–674, 1995.
- [41] Z. Tang, G. Blacquiere, and G. Leus, "Aliasing-free wideband beamforming using sparse signal representation," *IEEE Trans. Sig. Proc.*, vol. 59, no. 7, pp. 3464–3469, Jul. 2011.
- [42] A. Paulraj and T. Kailath, "Direction of arrival estimation by eigenstructure methods with imperfect spatial coherence of wave fronts," *J. Acoust. Soc. Am.*, vol. 83, pp. 1034–1040, 1988.
- [43] A. B. Gershman, C. F. Mecklenbrauker, and J. F. Bohme, "Matrix fitting approach to direction of arrival estimation with imperfect spatial coherence of wavefronts," *IEEE Trans. Sig. Proc.*, vol. 45, no. 7, pp. 1894–1899, Jul. 1997.
- [44] J. Ringelstein, A. B. Gershman, and J. F. Bohme, "Direction finding in random inhomogeneous media in the presence of multiplicative noise," *IEEE Sig. Proc. Letters*, vol. 7, no. 10, pp. 269–272, Oct. 2000.
- [45] M. Viberg and A. L. Swindlehurst, "Analysis of the combined effects of finite samples and model errors on array processing performance," *IEEE Trans. Sig. Proc.*, vol. 42, no. 11, pp. 3073–3083, Nov. 1994.
- [46] ———, "A Bayesian approach to auto-calibration for parametric array signal processing," *IEEE Trans. Sig. Proc.*, vol. 42, no. 12, pp. 3495–3507, Dec. 1994.